horticulturae

MDPI

Article

Integrated Omics Reveal Coordinated Defense Networks in *Annona squamosa* Against *Fusarium acutatum* Infection

Zhenyu An [1,†], Ruibin Kuang [2,3,4,†], Shuhuan Lin [5], Xing Long [1], Yuerong Wei [2,3,4], Yan Qin [1], Jinyan Yao [1], Jingmei Tang [6], Fangnan Kong [6], Wenzhong Tang [1], Weixiong Huang [1], Kai Yu [7], Ji Zhang [1,*] and Ren Fang [1,*]

1 Horticultural Research Institute, Guangxi Academy of Agricultural Sciences, Nanning 530007, China; anderlu0396@126.com (Z.A.); longxing80@126.com (X.L.); qinyan_42@foxmail.com (Y.Q.); jinyan.yao@gxaas.net (J.Y.); twz@gxaas.net (W.T.); hwxwt@126.com (W.H.)
2 Institute of Fruit Tree Research, Guangdong Academy of Agricultural Sciences, Guangzhou 510640, China; rbkuang15@163.com (R.K.); weid18@163.com (Y.W.)
3 Key Laboratory of South Subtropical Fruit Biology and Genetic Resource Utilization, Ministry of Agriculture and Rural Affairs, Guangdong Academy of Agricultural Sciences, Guangzhou 510640, China
4 Guangdong Provincial Key Laboratory of Science and Technology Research on Fruit Tree, Guangdong Academy of Agricultural Sciences, Guangzhou 510640, China
5 Zhejiang Xinong Chemical Sales Co., Ltd., Hangzhou 310021, China; linhuan_19823@163.com
6 Southwestern Institute of Subtropical Agriculture, Chongzuo 532406, China; tjm7123025@163.com (J.T.); nan.1988.an@163.com (F.K.)
7 Guangxi Key Laboratory of Efficacy Study on Chinese Materia Medica, Guangxi University of Chinese Medicine, Nanning 530200, China; bioneer@foxmail.com
* Correspondence: zhangji@gxaas.net (J.Z.); fangren1981@126.com (R.F.); Tel.: +86-0771-3245047 (R.F.)
† These authors contributed equally to this work.

Abstract

Root rot disease severely threatens tropical fruit production, leading to plant mortality and reduced yields; however, the mechanisms of host defense responses and pathogen infection remain poorly understood. In this study, *Fusarium acutatum* was isolated from diseased *Annona squamosa* roots and identified through morphological features and ITS phylogeny (99.8% identity). Infection triggered a marked activation of antioxidant defenses, with elevated POD, SOD, PAL, PPO, and CAT activities. Transcriptomic and TMT-based quantitative proteomic analyses identified 23,791 and 74,403 differentially expressed genes (DEGs) and 367 and 609 differentially expressed proteins (DEPs) in root at 5 and 10 days post inoculation, respectively, relative to the control. These DEGs and DEPs were consistently enriched in pathways involving redox regulation, protein synthesis and processing, ubiquitin-mediated proteolysis, phenylpropanoid and flavonoid metabolism, cell wall remodeling, plant–pathogen interaction and MAPK signaling. Integrated transcriptomic–proteomic correlation analysis showed clear positive associations between key defense-related genes and proteins, suggesting that phenylpropanoid metabolism and reactive oxygen species (ROS) scavenging play central roles in resistance. Key genes such as *CHI2*, *CHS*, and *CYP* were strongly induced and validated by qPCR, supporting coordinated activation of the defense systems. Furthermore, *F. acutatum* exhibited upregulation of 50 pathogenic-related proteins, including 4 cell wall-degrading enzymes (e.g., CBH1, pectate lyase), 5 metabolic regulation or signal transduction enzymes (e.g., gabD, TPI, and ENO) and 3 potential effectors, suggesting coordinated pathogen strategies for host colonization. Collectively, this study provides comprehensive multi-omics insight into the molecular mechanisms underlying *A. squamosa* defense against *F. acutatum* and offers candidate targets supported by omics evidence, serving as a theoretical reference for the management of root rot.

Check for updates

Academic Editor: Minjie Qian

Received: 19 November 2025
Revised: 19 December 2025
Accepted: 25 December 2025
Published: 28 December 2025

Copyright: © 2025 by the authors. Licensee MDPI, Basel, Switzerland. This article is an open access article distributed under the terms and conditions of the Creative Commons Attribution (CC BY) license.

Keywords: sugar apple; root rot disease; transcriptomic; proteomic; phenylpropanoid metabolism; antioxidant; cell wall-degrading enzymes

1. Introduction

Sugar apple (*Annona squamosa* L.) is a tropical fruit belonging to the order Magnoliales, family Annonaceae, and genus *Annona* [1]. It is highly valued for its distinctive flavor, rich nutritional profile, and multiple medicinal benefits, and is widely cultivated in southern China [2]. However, the commercial production of sugar apple is severely constrained by a range of biotic stresses. Among them, root rot represents one of the most destructive diseases, causing significant yield loss and quality decline [3]. The disease is predominantly caused by *Fusarium* spp., with *Fusarium acutatum* identified as the major pathogen responsible for root rot in sugar apple [3,4]. Infection typically initiates in the root cortex and progresses into the vascular tissue, leading to structural deterioration, compromised nutrient and water uptake, growth inhibition, and eventual plant death [5,6]. Therefore, understanding the plant's defense mechanisms in response to *F. acutatum* infection is crucial for developing effective control measures and guiding resistance breeding.

The infection process triggered by *Fusarium* in plants involves complex molecular interactions that activate a broad spectrum of host defense responses. One of the earliest responses is the initiation of antioxidant defense systems, including key enzymes such as peroxidase (POD), superoxide dismutase (SOD), phenylalanine ammonia-lyase (PAL), and catalase (CAT) [7]. These enzymes function cooperatively to scavenge excessive reactive oxygen species (ROS) generated during pathogen invasion, thereby mitigating oxidative damage [8]. Meanwhile, the phenylpropanoid metabolism pathway is rapidly induced, leading to the accumulation of lignin, flavonoids, and other secondary metabolites that reinforce the cell wall and restrict pathogen spread [9]. Signal transduction via mitogen-activated protein kinase (MAPK) cascades further amplifies defense responses by activating downstream stress-related transcription factors and resistance genes [10].

Plant hormonal signaling pathways also contribute to the defense networks against *Fusarium* infection. The salicylic acid (SA) pathway enhances the transcription of pathogenesis-related (PR) genes such as *PR1*, *PR2*, and *PR3*, which encode antifungal proteins that limit *Fusarium fujikuroi* colonization in rice [11]. Crosstalk among ethylene (ET), jasmonic acid (JA), and abscisic acid (ABA) signaling pathways fine-tunes the balance between growth and immunity, modulating root architecture and cellular homeostasis [12,13]. Concurrently, ROS generated by enzymes such as NADPH oxidase and POD function as both antimicrobial agents and secondary messengers for systemic immunity [14]. Reinforcement of the cell wall through elevated lignin and cellulose biosynthesis provides an additional physical barrier against *Fusarium graminearum* invasion [15], while systemic acquired resistance (SAR) ensures long-term defense activation throughout the plant [16].

Despite accumulating evidence regarding these defense processes, the molecular regulatory networks orchestrating *A. squamosa* responses to *F. acutatum* remain largely unexplored. Previous studies have mostly focused on individual defense components, lacking integrative analyses that connect transcriptional and translational responses. The complexity of *Fusarium* pathogenicity and its diverse infection strategies further complicate mechanistic interpretation. With the rapid advancement of high-throughput omics technologies, integrative approaches, especially transcriptomics and proteomics, have emerged as powerful tools for dissecting the molecular architecture of plant–pathogen interactions. By combining mRNA and protein expression analyses, it becomes possible to capture

both gene-level regulation and functional protein execution, thereby revealing coordinated defense networks.

In this study, we employed RNA sequencing and tandem mass tag (TMT)-based quantitative proteomics to investigate the dynamic responses of *A. squamosa* roots to *F. acutatum* infection at 0, 5 and 10 days post inoculation (dpi). Differentially expressed unigenes (DEGs) and proteins (DEPs) were identified and integrated with enzyme activity assays and physiological analyses to validate defense-associated trends. The objectives of this study were to unravel the transcriptional and translational regulation underlying *A. squamosa* defense responses, to identify candidate genes and protein networks associated with resistance, and to provide a molecular foundation for future breeding and disease management strategies in tropical fruit crops.

2. Materials and Methods

2.1. Collection of Diseased Plant Samples

Root samples exhibiting typical root rot symptoms were collected from *A. squamosa* orchards located in Guangxi and Guangdong, with five orchards (10~50 mu) selected for sampling in each province. Five representative diseased plants showing consistent and characteristic symptoms were selected for pathogen isolation. The affected roots, showing grayish or brown discoloration, were carefully excavated, rinsed with sterile distilled water, wrapped in sterile aluminum foil, and transported to the laboratory in sterile containers under chilled conditions.

2.2. Pathogen Isolation, Purification and Identification

Root segments were surface-sterilized with 75% ethanol for 30 s, followed by 1% NaClO for 1 min, and rinsed three times with sterile distilled water before plating. Pathogens were isolated and purified using a conventional tissue isolation method as described by Gautam et al. [17]. Representative pathogenic isolates were cultured on PDA at 28 °C for 7 days to examine colony morphology and hyphal characteristics under a light microscope (BX53, Olympus, Tokyo, Japan). For molecular identification, genomic DNA was extracted from purified isolates, and the internal transcribed spacer (ITS) region of rDNA was amplified using the universal primer pair ITS1 (5′-TCCGTAGGTGAACCTGCGG-3′) and ITS4 (5′-TCCTCCGCTTATTGATATGC-3′) [18]. PCR amplification was performed in a 20 μL reaction mixture containing 4 μL of 5× FastPfu Buffer, 0.8 μL of each primer, 2 μL of 2.5 mM dNTPs, 0.4 μL of FastPfu DNA polymerase (TransGen Biotech, Beijing, China), 0.2 μL of BSA, and approximately 10 ng of template DNA. PCR amplification was performed in an ABI 9700 thermocycler (Applied Biosystems, Foster City, CA, USA) under the following conditions: initial denaturation at 94 °C for 5 min; followed by 35 cycles of denaturation at 94 °C for 30 s, annealing at 56 °C for 45 s, and extension at 72 °C for 90 s; with a final extension at 72 °C for 10 min. The amplified products were visualized on 1.5% agarose gels and sequenced by Sangon Biotech (Shanghai, China). Sequence alignment and BLAST (2.11.0) analysis were performed against NCBI ITS database. Phylogenetic trees were constructed in MEGA10.0 using the Neighbor-Joining method with the Kimura 2-parameter model. Bootstrap analysis was conducted with 1000 replicates, and branch support was assessed based on bootstrap values to confirm taxonomic identity.

2.3. Preparation of Spore Suspension

For inoculation assays, three representative *Fusarium* isolates previously purified and maintained on potato dextrose agar (PDA; Huankai Microbial, Guangzhou, China) were used. Cultures were incubated at 28 °C for 12 days. Conidia formed on the culture surface

were gently washed off, and the resulting suspension was adjusted to a final concentration of 2×10^6 spores mL^{-1} for subsequent inoculation assays.

2.4. Inoculation Assay and Sample Collection

When *A. squamosa* seedlings were eight weeks old (2~3 true leaves), their roots were partially immersed in *F. acutatum* spore suspension, while sterile distilled water served as the control. After 15 min of immersion, seedlings were replanted in sterilized growth substrate (peat:perlite:leaf mold = 2:1:1, with 10% sterile river sand, pH 5.8~6.5) and maintained under controlled conditions (28 °C, 14 h light/10 h dark, and 75~80% humidity). Each treatment included 30 seedlings for phenotypic observation.

Following the technical guidelines for evaluating *A. squamosa* disease resistance (NY/T 2054-2011) [19], disease severity, disease index, and percentage of necrotic roots were assessed at different inoculation time points. Root samples were collected at 5 and 10 dpi, representing MR (mid-stage) and LR (late-stage), with uninoculated plants as CK (normal control). Root samples were collected, immediately frozen in liquid nitrogen, and stored at −80 °C until further analysis. Three seedlings per treatment were pooled for each of three biological replicates for transcriptomic and proteomic analyses, while biochemical parameters were measured in six individual seedlings.

2.5. Transcriptomic Analysis

Root samples were ground into a fine powder in liquid nitrogen, and total RNA was extracted using TRIzol reagent (Invitrogen, Carlsbad, NM, USA). Genomic DNA was removed with DNase I (TaKaRa, Kusatsu, Shiga, Japan). RNA integrity was assessed by agarose gel electrophoresis, while RNA quality was evaluated using a Nanodrop ND-2000 spectrophotometer (Thermo Fisher, Waltham, MA, USA) and an Agilent 2100 Bioanalyzer (Agilent Technologies, Santa Clara, CA, USA). Samples meeting the following quality criteria (OD260/280 = 1.8~2.2, OD260/230 $\geq$ 2.0, RIN $\geq$ 6.5, 28S:18S $\geq$ 1.0, and total RNA > 2 μg) were used for library construction. RNA-seq libraries were constructed using the TruSeq™ RNA Sample Preparation Kit (Illumina, San Diego, CA, USA) according to the manufacturer's protocol. The main steps were as follows: (1) mRNA enrichment using oligo(dT) magnetic beads; (2) fragmentation of mRNA into ~200 bp fragments; (3) reverse transcription of fragmented mRNA and synthesis of double-stranded cDNA; (4) end repair and adaptor ligation of cDNA fragments; and (5) PCR amplification and size selection of 200~300 bp products. Finally, high-throughput sequencing was performed on an Illumina HiSeq X platform (Illumina, San Diego, CA, USA).

2.6. Proteomic Analysis

Root samples were ground in liquid nitrogen, and total proteins were extracted with lysis buffer (8 M urea, 100 mM EDTA, 10 mM IAA, 1% PMSF). After centrifugation (12,000 rpm, 10 min, 4 °C), protein concentration was determined using a BCA assay kit (Thermo Fisher Scientific, Waltham, MA, USA). For TMT labeling, 100 μg of total protein per sample was reduced with 10 mM TCEP (37 °C, 1 h), alkylated with 40 mM IAA (RT, dark, 40 min), precipitated with acetone (−20 °C, 4 h), and digested with trypsin (1:50 overnight, followed by 1:100 for 6 h). Peptides were labeled with TMT 10-plex reagents (Thermo Fisher Scientific, Waltham, MA, USA), pooled, fractionated by high-pH reverse-phase HPLC into 10 fractions, vacuum-dried, and reconstituted for LC–MS/MS. Separation was performed on an UltiMate 3000 nanoLC coupled with an Orbitrap Exploris 480 mass spectrometer (Thermo Fisher Scientific, Bremen, Germany) using a C18 column (75 μm × 25 cm). The flow rate was 300 nL min^{-1} over a 120 min gradient (A: 2% acetonitrile, B: 80% acetonitrile, both with 0.1% formic acid). MS1 and MS2 resolutions were 70,000 and 35,000; MS scans covered m/z 350~1300 with the top 20 precursors fragmented (dynamic exclusion: 18 s).

2.7. Bioinformatics Analysis

Raw data preprocessing, functional annotation and enrichment of transcriptome and proteome were analyzed according to our previous study [20] with minor modifications. For transcriptome, raw paired-end reads were trimmed and quality-controlled using Fastp 0.23.0. Clean reads were assembled de novo with Trinity 2.10.0. Gene expression was quantified as reads counts and TPM using RSEM simulator, and DEGs between samples were identified with DESeq2 1.34.0 ($|\log2(\text{fold change})| > 1$ and FDR < 0.05). Proteomic raw MS files were analyzed using MaxQuant (1.5.2.8) against the transcriptome-annotated peptide database of *A. squamosa* and *F. acutatum*, with protein identification FDR < 0.01 and at least one unique peptide. DEPs were defined as fold change > 1.5 or <0.67 with $p < 0.05$. Gene functional annotation was performed against Nr, Swiss-Prot, KEGG, and GO databases using BLASTx (E-value < 1×10^{-5}). Mercator 3.6 was used for protein sequence annotation pipeline to map pathways [21]. MapMan 3.6 was used for pathway mapping of DEPs. Signal peptide prediction of fungal proteins was carried out using DeepSig [22].

2.8. Physiological and Biochemical Parameters

The determination of soluble sugar and soluble protein was measured following established protocols [23]. Enzyme activities were determined as follows: peroxidase (POD) via the guaiacol oxidation method, polyphenol oxidase (PPO) via the catechol oxidation method, superoxide dismutase (SOD) via nitroblue tetrazolium (NBT) photoreduction, phenylalanine ammonia-lyase (PAL) via L-phenylalanine deamination, catalase (CAT) via hydrogen peroxide decomposition, and malondialdehyde (MDA) via the thiobarbituric acid colorimetric method (Jiancheng Bioengineering, Nanjing, China). For each treatment, five biological replicates (individual seedlings) were used, and each assay was performed in triplicate using 50 mg of fresh tissue per replicate.

2.9. RT-qPCR Validation Analysis

The primers were designed using Primer Premier 3.0 and synthesized by Qinke Company (Kunming, China) (Table S1). RT-qPCR was performed using SYBR Premix Ex TaqTM (TaKaRa, Kusatsu, Shiga, Japan) kit and Roche Lightcycler® 480 fluorescence quantitative PCR instrument (Roche, San Francisco, CA, USA) to analyze gene expression levels and validate sequencing results. Each treatment consisted of three independent biological replicates, and each replicate was measured in triplicate. Relative gene expression levels were calculated using the $2^{-\Delta\Delta Ct}$ method with the *GAPDH* as the internal reference.

2.10. Statistical Analysis

All experiments were conducted with at least three biological replicates. Data were expressed as mean ± standard deviation (SD). Data were organized using Excel 2021, and statistical analyses were conducted with SPSS 26.0. Shapiro–Wilk tests for normality and Levene's tests for homogeneity of variance were applied prior to parametric testing. Data meeting these assumptions were analyzed by one-way ANOVA with Duncan's test; otherwise, the Kruskal–Wallis test was used. Differences were considered statistically significant at $p < 0.05$.

3. Results

3.1. Identification and Phylogenetic Assignment of the Pathogenic Fungus

The fungal isolate obtained from diseased *A. squamosa* roots grew moderately on PDA medium, forming colonies with radiating aerial mycelia. The aerial hyphae were moderately developed, and the conidiophores were monophialidic and hyphal in origin, producing abundant white conidia of hyphal origin. Numerous chlamydospores were

observed, mostly spherical to lemon-shaped, occurring either terminally or intercalarily. As the culture aged, the colony center gradually turned light yellowish-brow (Figure 1A). Microscopic observation revealed kidney- to oval-shaped microconidia (5.1~15.5 × 2.9~4.6 μm) and fusiform macroconidia, typically with one to three septa, exhibiting slightly curved apical cells (Figure 1B). PCR amplification of the ITS region produced a distinct 535 bp fragment. BLAST analysis of the sequence revealed 99.8% similarity with *F. acutatum*. Phylogenetic analysis clustered the isolate within the same clade as reference *F. acutatum* strains (Figure 1C). Based on the morphological characteristics and ITS sequence analysis, the pathogen was confirmed as *F. acutatum*. Disease progression was monitored during the 10 dpi. Five days post inoculation, dark brown spots appeared at root tips with leaf drooping, indicating early root infection. By 10 dpi, root lesions expanded and became water-soaked, with wilting and yellowing of lower leaves, indicating severe root dysfunction (Figure 1D).

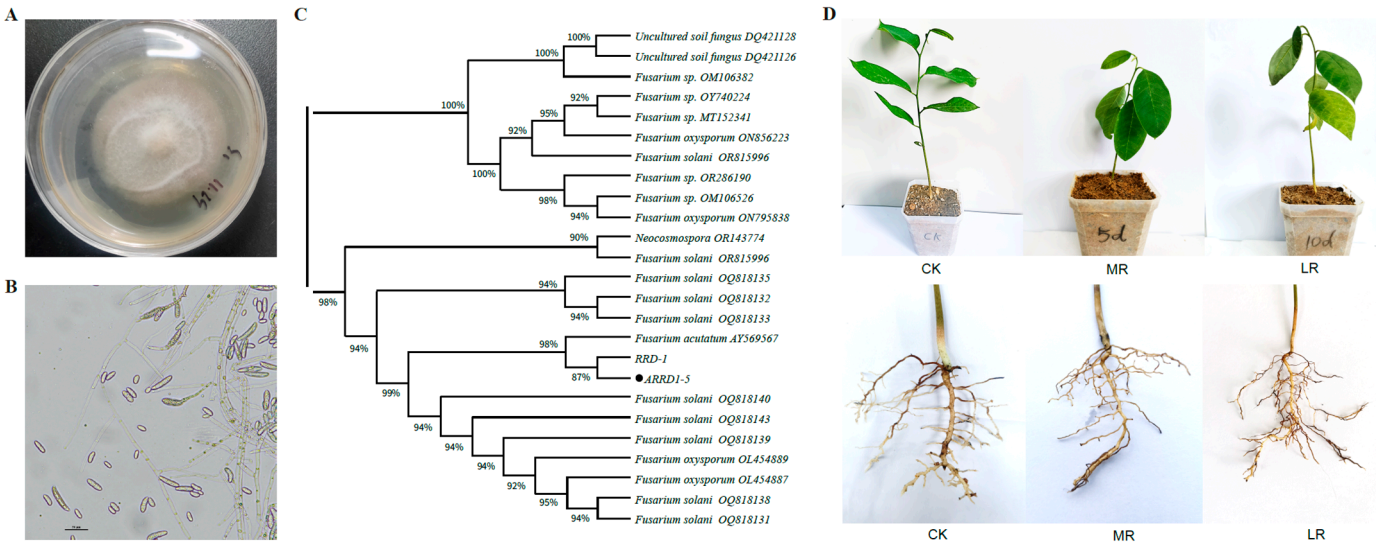


Figure 1. Morphology and phylogenetic tree of isolated *F. acutatum*. (**A**) Fungal morphology on PDA medium. (**B**) Morphology of hyphae and conodia of pathogenic fungus. Black dot indicates the fungal strains screened in this study. ARRD1–5, *Annona* root rot disease strains 1–5; RRD-1, a previously identified root rot disease strain (*F. acutatum*). (**C**) Phylogenetic tree analysis of root rot pathogens based on its ITS sequence. (**D**) Symptoms of *A. squamosa* infected by *F. acutatum*. Visual appearance of plant growth (**top**) and root morphology exhibiting typical damage (**bottom**) at various infection stages.

3.2. Overview of Transcriptomic Analysis

Quality control of RNA-sequencing data showed that each sample contained more than 6.0×10^9 bases, with sequencing error rates below 0.024% and Q30 values exceeding 95%, ensuring high sequencing accuracy and reliability (Table S2). Correlation analysis revealed strong intra-group reproducibility ($r > 0.99$), and closer similarity between CK and MR ($r > 0.96$) than between CK and LR ($r > 0.88$), consistent with progressive infection by *F. acutatum* (Figure 2A).

Principal component analysis (PCA) confirmed clear group separation and compact clustering within replicates (Figure 2B). A total of 205,097 unigenes were assembled. 23,791 DEGs were identified in MR vs. CK (21,601 upregulated and 2190 downregulated), 66,203 DEGs in LR vs. CK (61,219 upregulated and 4984 downregulated), and 74,403 DEGs in LR vs. MR (56,124 upregulated, 18,279 downregulated) (Figure 2C–E). Venn analysis showed 10,199 commonly upregulated and 1112 commonly downregulated DEGs between

MR vs. CK and LR vs. CK (Figure 2F), indicating that most infection-responsive genes remained persistently regulated at later stages.

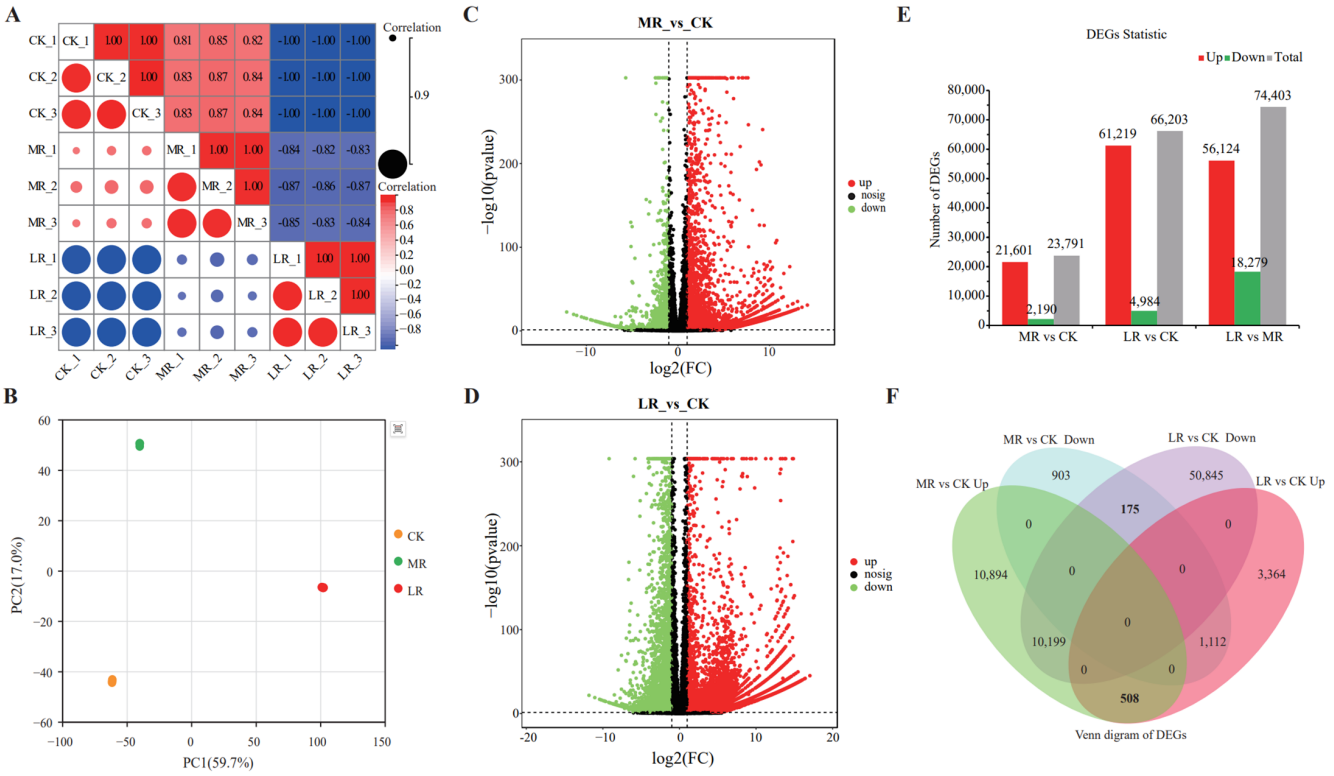


Figure 2. Overview of transcriptomic analysis results. (**A**) Sample correlation analysis. (**B**) Principal component analysis (PCA). (**C**) Volcano plot of differentially expressed genes (DEGs) in MR vs. CK. (**D**) Volcano plot of DEGs in LR vs. CK. (**E**) Statistics of DEGs among comparison groups; (**F**) Venn diagram of DEGs.

3.3. Functional Analysis of DEGs

GO and KEGG enrichment analyses were performed to elucidate the biological functions of DEGs. In MR vs. CK, GO_CC enrichment showed that DEGs were primarily localized to membrane components, mitochondrial membrane, extracellular region, and respiratory chain (Figure S1A). GO_MF enrichment revealed significant enrichment in oxidoreductase, monooxygenase, and hydrolase activity, as well as iron ion binding, unfolded protein binding, and transporter activity (Figure 3A). GO_BP enrichment indicated that DEGs were mainly involved in heat stress response, protein folding, abiotic stimulus response, and lipid biosynthetic processes (Figure S1B). In LR vs. CK, DEGs were predominantly enriched in GO_CC terms related to plasma membrane, endomembrane system, and extracellular region (Figure S1C), and GO_MF terms including protein binding, oxidoreductase, monooxygenase, nucleic acid binding, transcription factor, and iron ion binding (Figure 3B). GO_BP enrichment showed that DEGs mainly participated in stress responses, responses to oxygen-containing compounds, and defense-related biological processes (Figure S1D).

KEGG analysis revealed that DEGs in MR vs. CK were enriched in protein processing in the endoplasmic reticulum, ubiquitin-mediated proteolysis, starch and sucrose metabolism, terpenoid biosynthesis, plant–pathogen interaction, ABC transporters, N-glycan biosynthesis, and several amino acid metabolism pathways (Figure 3C). Metabolism-related pathways mainly associated with carbon, amino acid, energy, lipid, and secondary metabolite metabolism, whereas genetic information processing pathways were related to protein folding, sorting and degradation, translation, and transcription. Cellular process-

related pathways were primarily involved in transport and catalytic activity (Figure S1E). In LR vs. CK, enriched pathways included ubiquitin-mediated proteolysis, flavonoid biosynthesis, phenylpropanoid biosynthesis, plant hormone signal transduction, protein processing in the endoplasmic reticulum, MAPK signaling, and ribosome-related pathways (Figure 3D). Similarly, metabolism-related pathways encompassed carbon, amino acid, energy, lipid, and secondary metabolism, while genetic information processing pathways were associated with translation, folding, sorting and degradation, and transcription. Pathways related to cellular processes were mainly linked to transport and catalytic activity (Figure S1F).

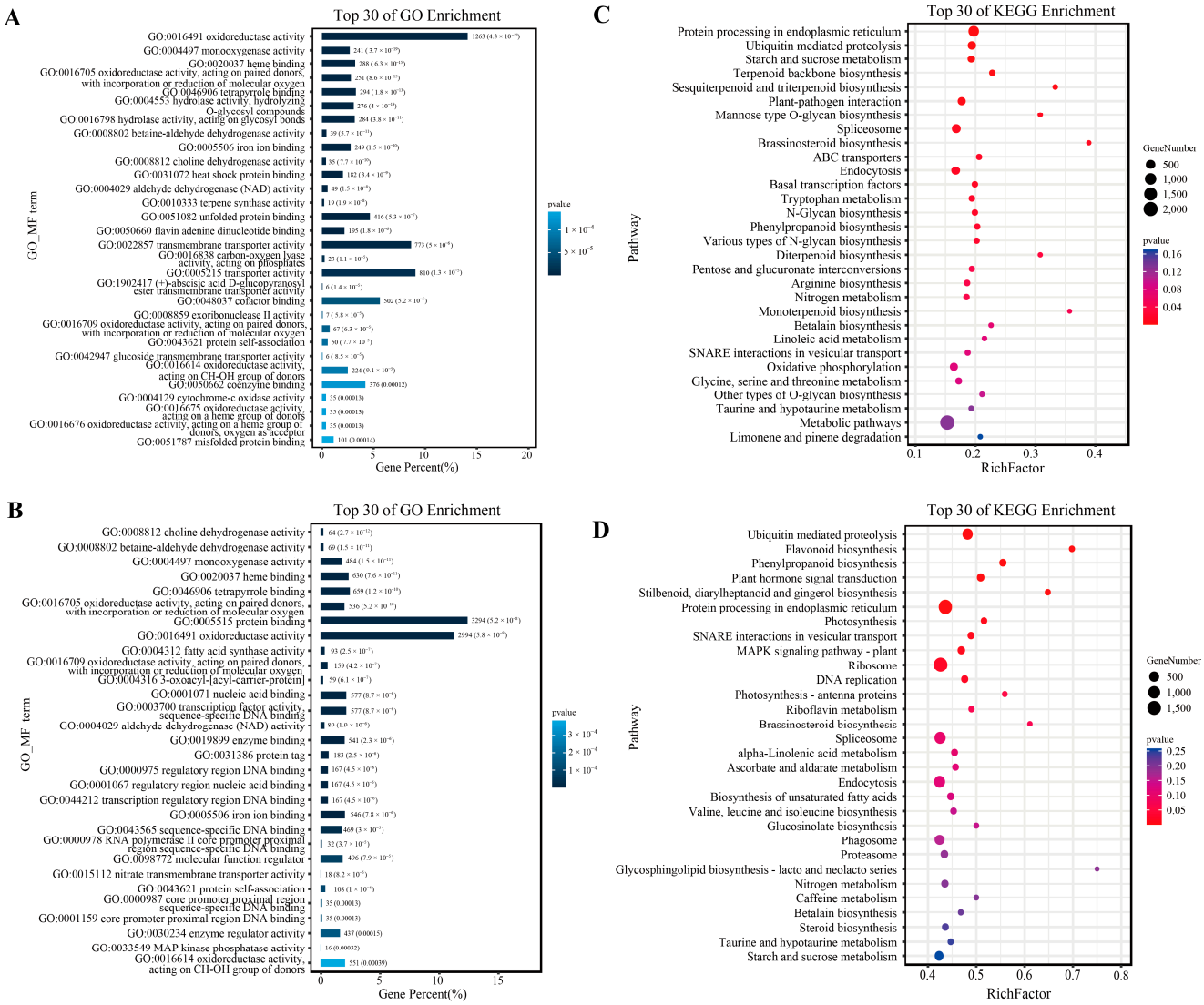


Figure 3. Functional enrichment analysis of DEGs based on GO and KEGG. (**A**) GO_MF statistics and enrichment of DEGs in MR vs. CK. (**B**) GO_MF statistics and enrichment of DEGs in LR vs. CK. (**C**) KEGG pathway enrichment of DEGs in MR vs. CK. (**D**) KEGG pathway enrichment of DEGs in the LR vs. CK. Each panel presents the top 30 significantly enriched GO or KEGG pathways, ranked by *p* value.

3.4. Overview of Proteomic Analysis Results

Proteomic correlation analysis revealed good reproducibility among biological replicates ($r > 0.5$) for all samples except LR_2, indicating good quantitative reproducibility. Nevertheless, LR_2 was retained in all subsequent analyses, as it met the predefined quality control criteria and did not show abnormal behavior in global proteomic distribution.

Intergroup correlations showed that the CK and MR exhibited higher similarity, whereas the correlation between CK and LR was much lower ($r \leq 0.1$), suggesting a progressive divergence of the proteome as infection advanced. This pattern corresponded well to the different infection stages of *Fusarium* (Figure 4A). PCA confirmed distinct separation among CK, MR, and LR groups, while samples within each group clustered closely together, confirming the high reproducibility of biological replicates (Figure 4B). Totally, 367 DEPs were identified in MR vs. CK (294 upregulated, 73 downregulated) and 609 DEPs in LR vs. CK (330 upregulated, 279 downregulated). 434 DEPs were detected in LR vs. MR, including 203 upregulated and 231 downregulated proteins (Figure 4C–E). Venn diagram analysis of MR vs. CK and LR vs. CK comparisons revealed that 89 upregulated proteins and 51 downregulated proteins were shared between the two groups (Figure 4F), indicating a sustained defense-related proteomic response across infection stages.

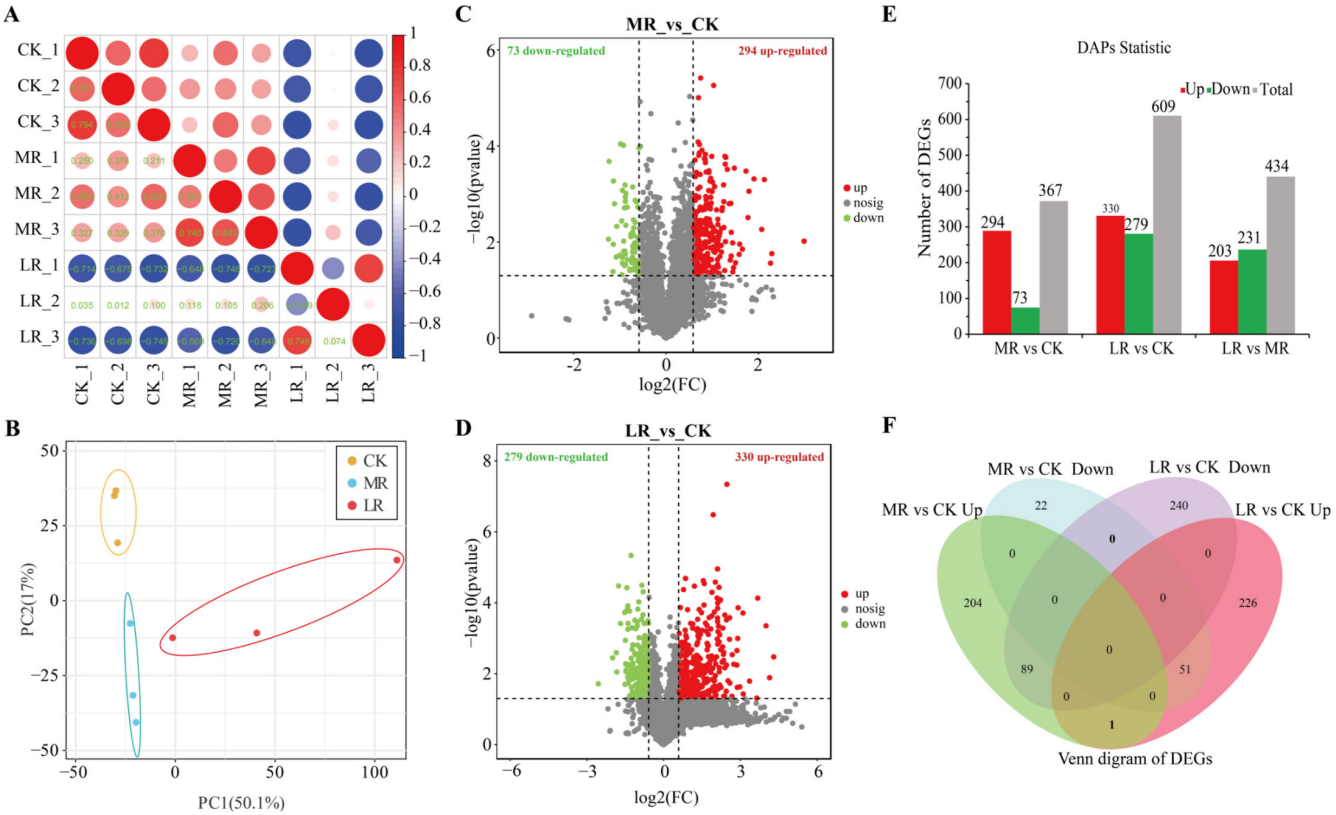


Figure 4. Overview of proteomic analysis results. (**A**) Sample correlation analysis. (**B**) Principal component analysis (PCA). (**C**) Volcano plot of DEPs in MR vs. CK. (**D**) Volcano plot of DEPs in LR vs. CK. (**E**) Statistics of DEPs among comparison groups. (**F**) Venn diagram of DEPs.

3.5. Functional Analysis of DEPs

GO enrichment revealed that DEPs in MR vs. CK were mainly localized to cellular membranes, involved in transporter, oxidoreductase, and ATPase activity, and associated with transmembrane transport and related biological processes (Figure S2A). In LR vs. CK, DEPs were most enriched in ribosomes, and associated with ribosomal complexes and translation-related functions (Figure S2B). Expression clustering of all DEPs revealed strong within-group consistency, while intergroup comparisons showed that CK and MR were closely related, whereas LR was more distinct, indicating greater proteomic divergence at the late infection stage. The DEPs were categorized into seven expression patterns (Figure 5A). Among these, clusters 0, 3, 4, and 7 exhibited significant aggregation. Specifically, proteins in Cluster 0 showed a gradual decrease in expression (75 proteins), Cluster 3 proteins remained stable initially and then decreased (37 proteins), Cluster 4 pro-

teins remained unchanged initially and then increased (261 proteins), and Cluster 7 proteins displayed a continuous increase in expression (78 proteins) (Figure 5B). The GO enrichment of specific proteins included in each cluster are presented in Figure 5C. Proteins with continuously increased expression (Clusters 4 and 7) were mainly associated with oxidation–reduction processes, ROS metabolism, translation, and oxidoreductase, catalase, and ribosomal structural activities, indicating enhanced redox regulation and protein synthesis during infection. Proteins in Cluster 3, which declined during infection, were enriched in translational elongation, peptide biosynthesis, protein folding, and cell wall organization. Proteins in cluster 0, showing gradual downregulation, were linked to ribosomal biogenesis, respiratory chain assembly, and chitin metabolism.

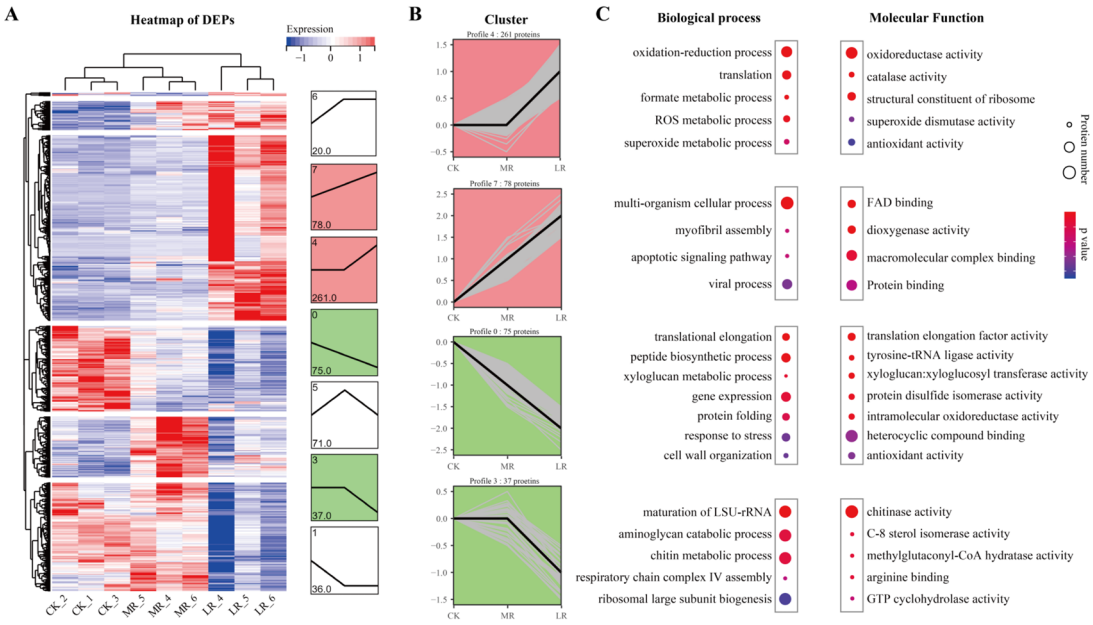


Figure 5. Trend analysis of DEPs. (**A**) Hierarchical clustering heatmap of DEPs. (**B**) Expression trend clustering of DEPs. (**C**) Detailed view of protein expression clusters.

KEGG pathway analysis indicated that MR vs. CK DEPs were enriched in tryptophan, lipid degradation, phenylpropanoid biosynthesis, and multiple carbohydrate metabolism, while LR vs. CK DEPs were mainly involved in ribosome biogenesis, aminoacyl-tRNA biosynthesis, protein processing in the endoplasmic reticulum, aminoacyl-tRNA biosynthesis, phenylpropanoid and flavonoid biosynthesis (Figure S2C,E). The DEPs were mapping into the catalytic processes and illustrate in the phenylpropanoid pathway (Figure S2D,F). MapMan visualization highlighted that defense-related DEPs were concentrated in processes such as cell wall remodeling, proteolysis, redox regulation (PODs, GSTs), hormone signaling (auxin, ethylene, JA), and pathogenesis-related (PR) proteins (Figure S3A,B). These findings indicate coordinated activation of structural, oxidative, and signaling pathways in *A. squamosa* during fungal infection.

3.6. Correlation Between Transcriptome and Proteome

Integrated multi-omics analysis demonstrated a significant positive correlation between unigene and protein expression, with Pearson's *r* increasing from 0.2743 in MR vs. CK to 0.6585 in LR vs. CK. In MR vs. CK, 157 unigenes/proteins were consistently upregulated and 7 were consistently downregulated among the 367 DEPs. In LR vs. CK, 297 unigenes/proteins showed consistent upregulation and 86 showed consistent downregulation among the 609 DEPs. Among these, the ten highlighted genes or proteins exhibiting higher correlation showed consistent and stable expression across both

comparison groups (Figure 6A,B). KEGG co-enrichment analysis revealed convergence in ubiquitin-mediated proteolysis, phenylpropanoid and flavonoid biosynthesis, MAPK signaling, and protein processing in the endoplasmic reticulum (Figure 6C). These results suggest progressive synchronization between transcriptional and translational defense responses as infection advances.

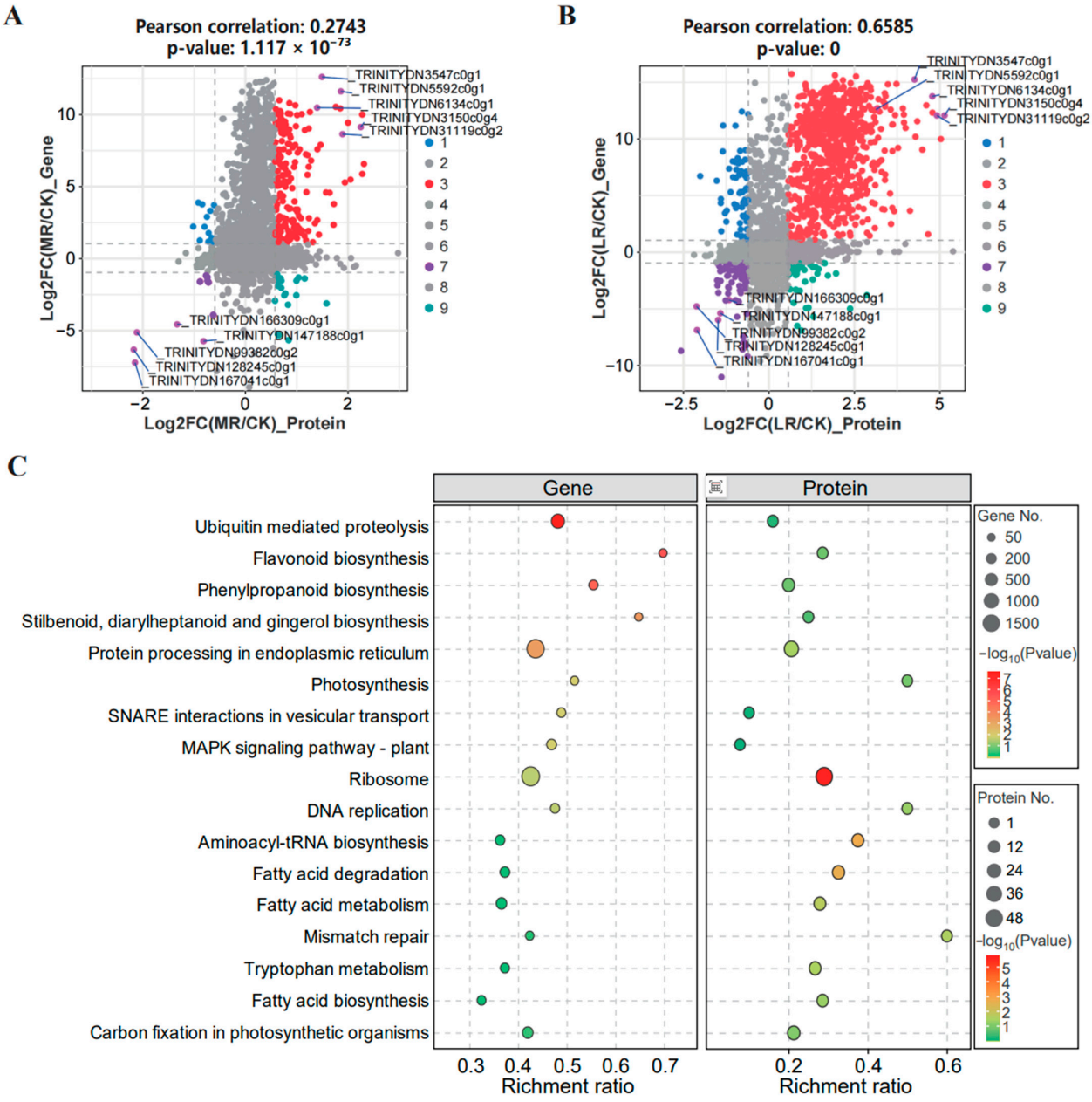


Figure 6. Correlation analysis between transcriptome and proteome. (**A**) Correlation analysis of unigene and protein expression levels in MR vs. CK. (**B**) Correlation analysis of unigene and protein expression levels in LR vs. CK. (**C**) Integrated KEGG pathway enrichment of DEGs and DEPs in LR vs. CK.

3.7. Changes in Antioxidant and Defense Enzyme Activities During Infection

Fungal infection induced pronounced modulation of antioxidant enzymes in *A. squamosa*. A total of 13 DEGs (11 upregulated and 2 downregulated) were annotated with the MF: superoxide dismutase activity in MR vs. CK and 37 DEGs (all upregulated) were annotated with MF: superoxide dismutase activity in LR vs. CK. For peroxidase activity, 54 DEGs (51 upregulated and 3 downregulated) were identified in MR vs. CK, and 146 DEGs (120 upregulated and 26 downregulated) in LR vs. CK. Among these, E1.11.1.7 represented

the most frequently enriched KEGG ortholog. Genes related to MF: phenylalanine ammonia-lyase activity were also notably responsive: 2 DEGs (both upregulated) were detected in MR vs. CK, and 18 DEGs (17 upregulated and 1 downregulated) in LR vs. CK, with 15 of them annotated as PAL in both stages. Similarly, genes associated with MF: catalase activity exhibited strong induction, with 6 DEGs (all upregulated) in MR vs. CK and 18 DEGs (16 upregulated and 2 downregulated) in LR vs. CK, indicating an elevated capacity for hydrogen peroxide decomposition. In contrast, polyphenol oxidase–related genes were relatively few, with 2 upregulated DEGs in MR vs. CK and 4 down-regulated in LR vs. CK (Figure 7A).

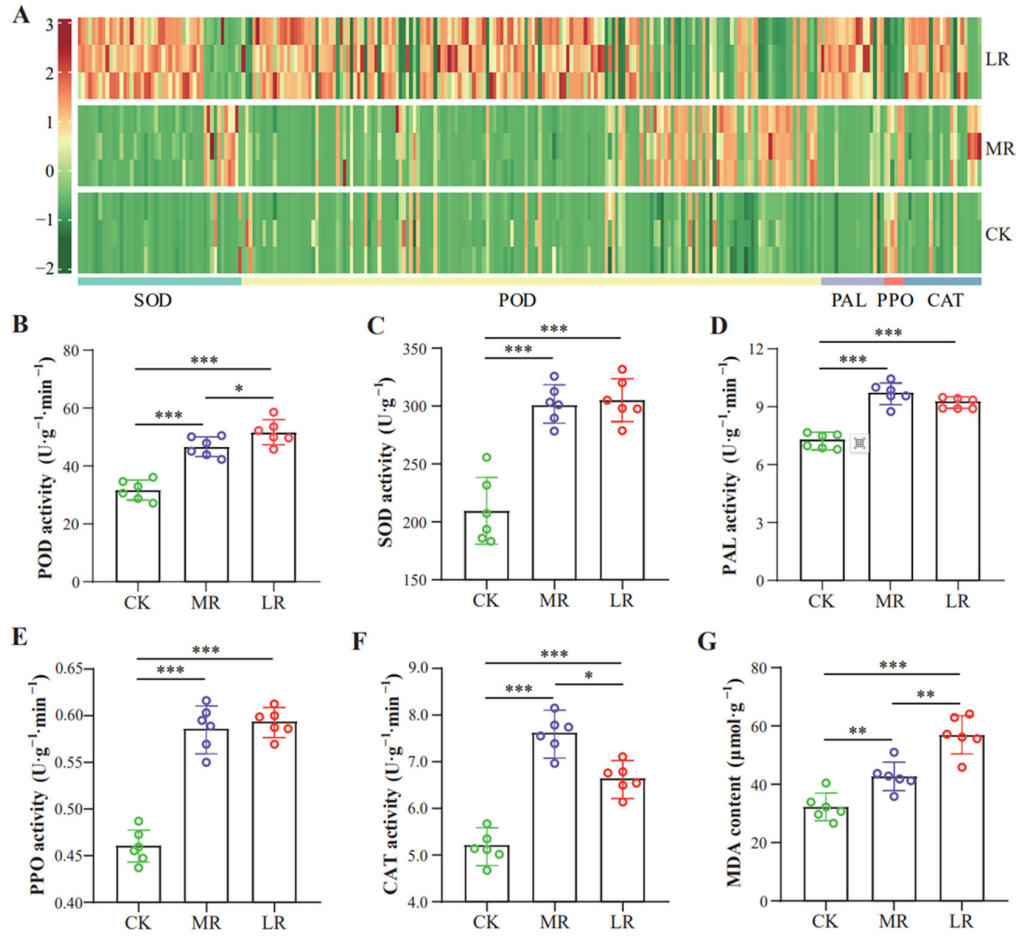


Figure 7. Antioxidant and defense enzyme activities during infection. (**A**) Heatmap of DEGs annotated to antioxidant enzyme activities. (**B**) POD activity. (**C**) SOD activity. (**D**) PAL activity. (**E**) PPO activity. (**F**) CAT activity. (**G**) MDA content. Data represent mean ± SD (n = 6). Statistical analysis was performed using one-way ANOVA followed by Duncan's test. * $p < 0.01$; ** $p < 0.01$; *** $p < 0.001$.

Correspondingly, POD activity at MR and LR was 45.52% and 56.94% higher than that of the CK, reaching its maximum at LR (Figure 7B). SOD activity increased by 43.37% and 41.36% at MR and LR, respectively, and remained stably high during infection (Figure 7C). PAL activity rose by 27.94% and 21.66% at MR and LR, showing strong early activation and sustained elevation (Figure 7D). PPO activity increased by 23.91% and 26.09% at MR and LR, respectively, with no significant difference between the two treatments (Figure 7E). CAT activity sharply increased to 7.63 $U \cdot g^{-1} \cdot min^{-1}$ at MR, 45.89% and 14.91% higher than CK and LR groups, respectively; although slightly reduced at LR, it was still 26.96% above CK, suggesting an early peak followed by a maintained high level (Figure 7F). In contrast, MDA content progressively accumulated during infection, increasing by 38.24% and 62.71% at

MR and LR, respectively, relative to CK, suggesting enhanced lipid peroxidation under fungal stress (Figure 7G). Overall, *F. acutatum* infection induced a pronounced antioxidant response in *A. squamosa*, characterized by enhanced POD, PPO, PAL, SOD, and CAT activities, accompanied by progressive lipid peroxidation.

3.8. Changes in Protein Procession and Sugar Metabolism During Infection

As illustrated in Figure 8A, fungal infection induced notable transcriptional reprogramming of genes involved in RNA and protein synthesis in *A. squamosa*. A large number of genes related to plastidic and cytosolic translation, ribosomal proteins, and aminoacyl-tRNA biosynthesis were significantly upregulated during both the MR and LR infection stages, suggesting an enhanced demand for protein synthesis to support defense and repair processes. As shown in Figure 8B, fungal infection also strongly modulated carbohydrate metabolism and cell wall precursor biosynthesis. Key intermediates of the sucrose–UDP-glucose pathway, including glucose-6-phosphate, fructose-6-phosphate, UDP-glucose, and UDP-galactose, were significantly upregulated, indicating enhanced flux through primary carbohydrate metabolism and cell wall polysaccharide synthesis. The activation of these pathways likely contributes to cell wall reinforcement and energy supply during pathogen challenge. Consistent with the transcriptomic changes, the biochemical assays demonstrated significant increases in soluble protein and soluble sugar contents (Figure 8C,D). Compared with CK, soluble protein content increased sharply at MR and remained relatively high at LR ($p < 0.001$), while soluble sugar content showed a similar pattern, peaking at MR ($p < 0.01$). These results collectively indicate that *F. acutatum* infection triggers an early burst of protein synthesis and carbohydrate metabolism, which may play crucial roles in maintaining cellular homeostasis, strengthening structural defenses, and supporting the energetic demands of stress responses.

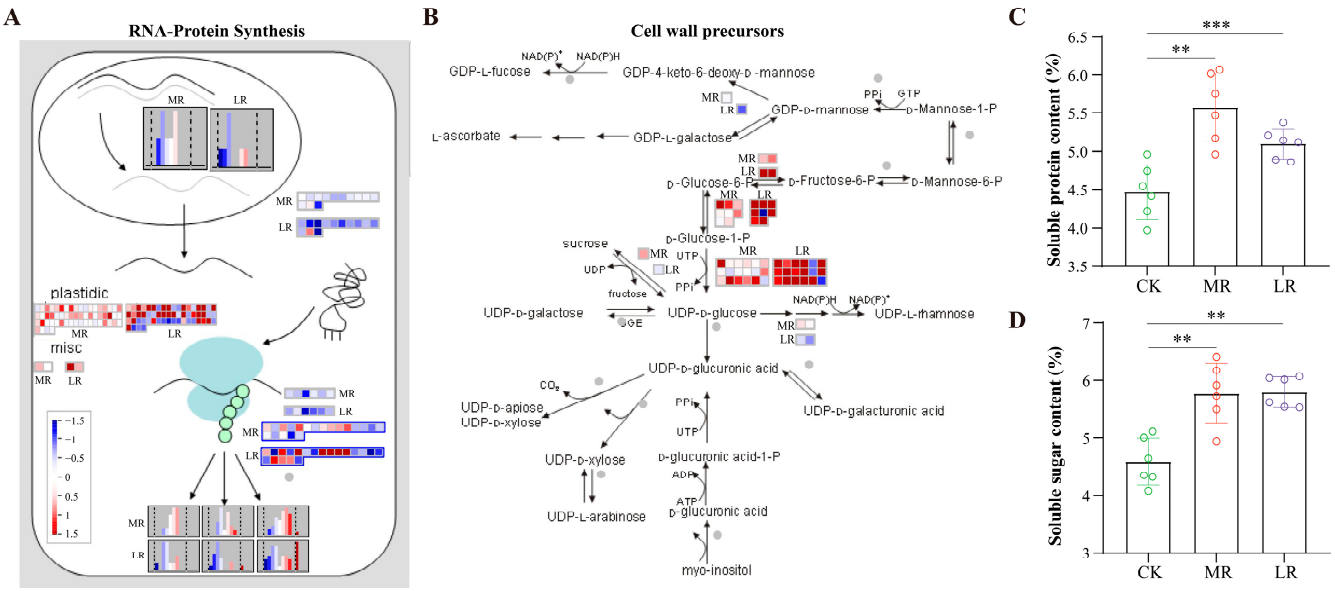


Figure 8. Changes in protein synthesis and sugar metabolism during fungal infection in *A. squamosa*. (**A**) Schematic representation of DEGs related to RNA and protein synthesis. (**B**) Schematic representation of DEGs involved in carbohydrate metabolism and cell wall precursor biosynthesis pathways. (**C**) Soluble protein content. (**D**) Soluble sugar content. Data represent mean ± SD ($n = 6$). Red and blue modules represent up- and downregulated proteins, respectively. Statistical analysis was performed using one-way ANOVA followed by Duncan's test. ** $p < 0.01$; *** $p < 0.001$.

3.9. Changes in Phenylpropanoid and Flavonoid Metabolism During Infection

F. acutatum infection triggered a marked reprogramming of secondary metabolism in *A. squamosa*, particularly within the phenylpropanoid and flavonoid biosynthetic pathways (Figure S4A,B). Comparative proteomic mapping revealed substantial enrichment of DEPs associated with phenylpropanoid metabolism in both MR vs. CK and LR vs. CK groups, suggesting a sustained activation of lignin and phenolic compound biosynthesis throughout infection. At the mid-stage of infection, several enzyme classes in the phenylpropanoid pathway, including PAL, POD, 4-coumarate-CoA ligase (4CL), cinnamyl-alcohol dehydrogenase (CAD), hydroxycinnamoyl-CoA:shikimate hydroxycinnamoyl transferase (HCT), and Catechol-O-Methyltransferase (COMT) were significantly upregulated (Figure S4C). This indicates the initiation of lignin polymerization and enhanced synthesis of phenolic intermediates involved in pathogen defense. At the late stage, these enzymes remained elevated, accompanied by the induction of flavonoid biosynthetic enzymes such as chalcone synthase (CHS), chalcone isomerase (CHI), and flavanone 3-hydroxylase (F3H) (Figure S4D) reflecting the activation of flavonoid-mediated antioxidant and antimicrobial defenses. Four genes from the *CHI*, *CHS*, and *CYP* families were validated by qPCR, and their expression trends were consistent with the omics data (Figure S4E).

3.10. Protein Expression Analysis of Fusarium acutatum During Infection

A total of 50 *F. acutatum*-derived proteins were significantly altered in LR vs. CK (Table S3). Among them, several categories of proteins were markedly upregulated, particularly fungal ribosomal proteins (RPL13A, RPS7), metabolism-related enzymes (gabD, TPI, ENO), and cell wall-degrading enzymes (CWDEs, e.g., CBH1) (Figure 9A). GO_MF enrichment analysis of the significantly upregulated proteins revealed that, as infection progressed, proteins associated with ribosomal structural components, oxidoreductase activity, hydrolase activity, and lyase activity were significantly enriched (Figure 9B). A detailed list of the upregulated proteins (4 CWDEs; 5 metabolic regulation or signal transduction, MRST; 3 potential effectors; 1 oxidative stress and host defense evasion) that might be involved in pathogen–host interaction is provided in Table 1.

Table 1. Candidate *F. acutatum* proteins potentially involved in host interaction.

ID	Accession	Protein Name	Log2FC (MR/CK)	Log2FC (LR/CK)	KO	Potential Function
rna1739	EWY93906.1	exoglucanase type C	2.49	4.10	K01225	CWDE
rna3759	KNB03063.1	pectate lyase	—	2.15	—	CWDE
rna12552	EXK41545.1	beta-glucosidase	—	1.44	K01188	CWDE
rna18786	CCT69715.1	alpha-N-arabinofuranosidase	—	1.16	—	CWDE
rna25156	KNB12728.1	catalase-peroxidase	0.73	1.48	K03782	Oxidative stress and host defense evasion
rna11528	EWY99219.1	NADP-specific glutamate dehydrogenase	—	1.56	K00262	MRST
rna3245	KNA95921.1	isocitrate lyase	—	1.12	K01637	MRST
rna15985	EWY91144.1	isocitrate lyase	—	1.09	K01637	MRST
rna8730	EWZ02163.1	formate dehydrogenase	—	1.84	K00122	MRST
rna21541	KNB11560.1	alcohol dehydrogenase	—	1.96	—	MRST
rna13312	KNA98200.1	hypothetical protein FOXG_02605	—	0.60	—	Potential effector
rna24563	EXK35733.1	hypothetical protein FOMG_08942	1.29	2.32	—	Potential effector
rna22058	EGU78729.1	hypothetical protein FOXB_10756	—	1.37	—	Potential effector

Note: CWDEs, Cell wall-degrading enzymes; MRST, Metabolic regulation or signal transduction.

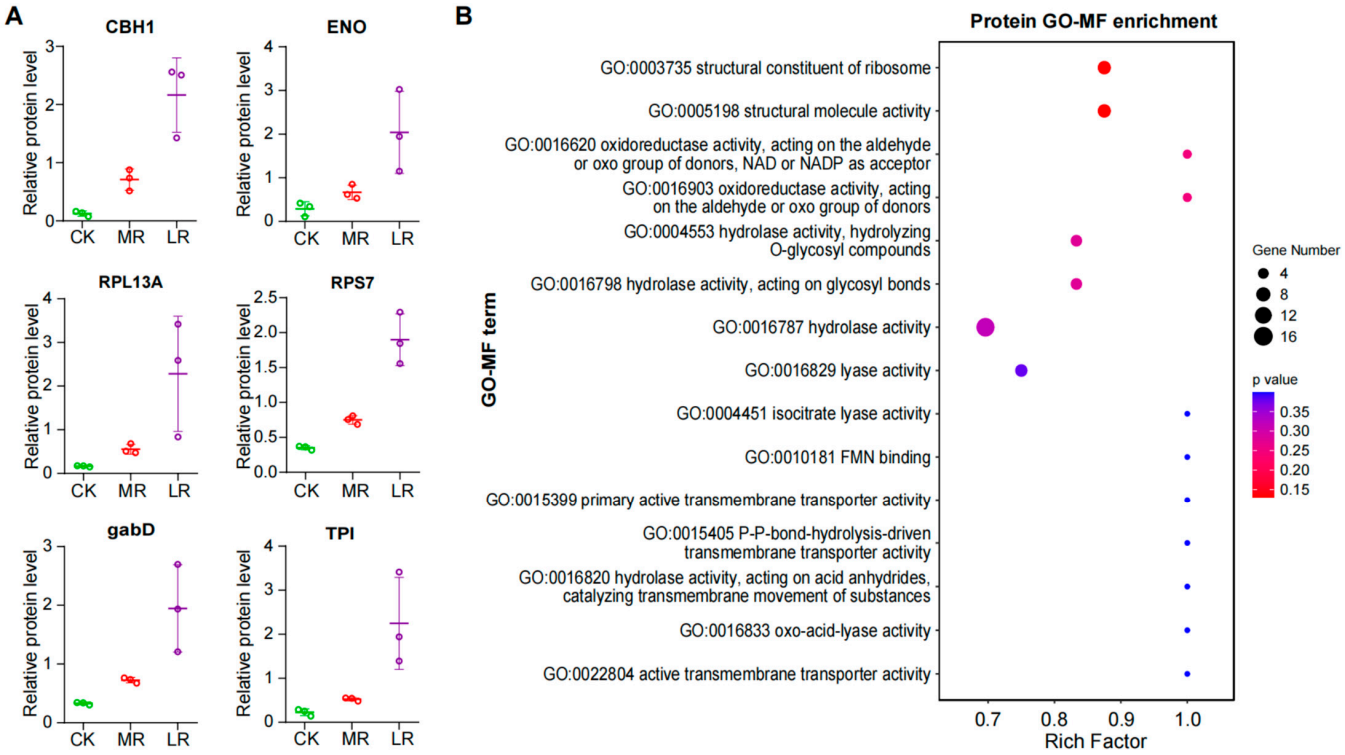


Figure 9. Protein expression analysis of *F. acutatum* during infection. (**A**) Expression cell wall–degrading enzymes (CBH1), ribosomal proteins (RPL13A, RPS7), metabolism-related enzymes (gabD, TPI, ENO). (**B**) GO_MF enrichment analysis of the DEPs.

4. Discussion

This study provides insights into the molecular defense mechanisms of *A. squamosa* against *F. acutatum* root rot, a major disease affecting tropical fruit production. Through integrated transcriptomic and proteomic analyses, key genes and proteins associated with host defense were systematically identified. Correlation analysis revealed a progressive increase in unigene–protein concordance from the MR to LR (MR, $r = 0.2743$; LR, $r = 0.6585$) (Figure 6A,B), indicating that as infection progressed, transcriptional and translational regulation became more closely associated. Such coordination likely supports a sustained and efficient immune response. The combined data highlight redox regulation, phenylpropanoid metabolism, and cell wall reinforcement as central defense axes. Understanding these coordinated pathways provides a reference for developing molecular strategies to enhance resistance and manage root rot in *A. squamosa*.

4.1. Cell Wall Reinforcement as a Primary Defense Barrier

The plant cell wall represents the first structural defense against pathogen invasion, and its remodeling capacity is critical to disease resistance. *Fusarium* species typically secrete diverse CWDEs to disrupt host cell wall architecture and facilitate colonization [24]. In *A. squamosa*, infection by *F. acutatum* was accompanied by pronounced signs of cell wall reinforcement, characterized by increased lignin deposition and upregulation of wall biosynthesis-related proteins (Figures S3 and S4). Elevated activities of PAL, POD, and phenolic compound synthases are consistent with enhanced lignin accumulation, which could form a more rigid barrier that may restrict fungal entry [25]. Simultaneously, altered polysaccharide composition and cross-linking with phenolic compounds likely contribute to wall stability and enzymatic resistance. Peroxidases appeared to be active in phenolic polymerization, potentially contributing to a dense, highly cross-linked wall matrix. Moreover, transcriptomic evidence suggests activation of wall-associated signaling and

hormone-mediated regulation (Figure 3). Recognition of *F. acutatum*-derived pathogen-associated molecular patterns (PAMPs) by plant pattern-recognition receptors (PRRs) likely triggered PAMP-triggered immunity (PTI), stimulating structural gene expression and accelerating wall repair. Plant hormones such as JA and ethylene (ET) may function synergistically in this process, modulating enzyme activities and integrating wall remodeling with immune signaling [26,27]. Collectively, cell wall reinforcement constitutes a key structural and biochemical strategy of *A. squamosa* against *F. acutatum*, achieved through coordinated lignification, polysaccharide cross-linking, and signal-regulated remodeling.

4.2. Activation of Antioxidant and Redox Defense Systems

ROS function as both cytotoxic molecules and crucial defense signals in plant–pathogen interactions [28,29]. Upon infection, *A. squamosa* exhibited pronounced activation of its antioxidant defense, as reflected by significantly increased activities of several defense-related enzymes, including POD, SOD, CAT, PPO, and PAL (Figure 7). This response indicates rapid re-establishment of redox homeostasis under pathogen-induced oxidative stress. At early infection stages, coordinated induction of SOD and CAT would facilitate detoxification of superoxide radicals and hydrogen peroxide, preventing uncontrolled oxidative damage [30,31]. Peroxidase-related genes (E1.11.1.7) were highly enriched in the KEGG annotation, highlighting the contribution of class III peroxidases to both ROS scavenging and wall strengthening. Concurrently, PAL activation provided precursors for lignin biosynthesis and other phenylpropanoid-derived defenses [31,32]. Transcriptomic enrichment of genes encoding oxidoreductases, monooxygenases, and iron ion-binding proteins (Figure 3) aligns with proteomic evidence showing elevated expression of oxidoreductases and peroxidases (Figure S1), suggesting that the host rapidly establishes an efficient ROS-scavenging and redox signaling system in response to invasion. Furthermore, KEGG pathway enrichment revealed significant involvement of MAPK signaling, protein processing in the endoplasmic reticulum, and ubiquitin-mediated proteolysis (Figure 6C), implying that redox homeostasis is closely linked to kinase signaling and protein quality control during infection. In summary, *A. squamosa* might employ a dynamic redox regulatory system to balance ROS production and detoxification, thus limiting pathogen spread and sustaining immune activation.

4.3. Maintenance of Protein and Sugar Homeostasis Under Stress

In addition to redox and structural defenses, maintaining protein and carbohydrate homeostasis is essential for sustaining metabolic balance under pathogen stress. Pathogen invasion imposes multiple physiological stresses, such as oxidative stress and metabolic disruption, prompting plants to reprogram protein synthesis, folding, and degradation processes while coordinating energy metabolism to support immune activation [33,34]. During infection, *A. squamosa* exhibited a marked induction of stress-responsive proteins, including antioxidant proteins, heat shock proteins (HSPs), and PR proteins (Figure S3A,B). Transcriptomic enrichment in endoplasmic reticulum protein processing, ubiquitin-mediated proteolysis, and HSP folding pathways (Figure 3C) suggests an enhanced capacity to counter infection-induced misfolding stress. Proteomic data confirming regulation of ribosomal proteins, translation initiation factors, and molecular chaperones (Figure S2), support the presence of an active proteostasis network. Additionally, the total soluble sugar accumulated markedly during infection (Figure 8D), which could provide metabolic energy and signaling functions that enhance antioxidant activity and defense gene expression [35]. Integrated omics analyses revealed enrichment of pathways related to carbon fixation and protein processing (Figure 6C), suggesting that *A. squamosa* reallocates resources to maintain energy supply and cellular homeostasis during infection. Together, these processes form a

coordinated proteostasis-sugar regulation network that stabilizes metabolism and supports sustained immune responsiveness under *F. acutatum* stress.

4.4. Activation of Phenylpropanoid and Flavonoid Metabolism

The phenylpropanoid and its downstream flavonoid biosynthetic pathways play pivotal roles in tropical fruits and vegetables responding to *Fusarium* infection. Numerous studies have demonstrated that these secondary metabolic routes contribute to plant defense at multiple levels by reinforcing the cell wall, scavenging reactive oxygen species, and producing antimicrobial compounds [36–38]. In *A. squamosa*, pathway mapping showed a broad upregulation of proteins involved in phenylpropanoid and flavonoid biosynthesis, promoting the biosynthesis of phenolic compounds and lignin (Figure S4). Transcriptomic and proteomic enrichment analyses revealed robust activation of these pathways following *F. acutatum* infection (Figure S4). Key enzymes including PAL, C4H, 4CL, COMT, and POD were upregulated, promoting phenolic compound accumulation and lignin polymerization. Flavonoid-related enzymes such as F3H and FLS were also induced, suggesting enhanced biosynthesis of antioxidant secondary metabolites [37,39–42]. The increased enzymatic activities of PAL and POD were consistent with the transcriptional and proteomic upregulation of phenylpropanoid-related genes and proteins, supporting the inference of enhanced flux through the phenylpropanoid pathway upon infection. Such an activation pattern may facilitate lignin deposition and cross-linking among cell wall components, thereby potentially strengthening the physical barrier and restricting pathogen invasion. In addition, upregulation of ABC transporters and genes related to the synthesis of defense-associated secondary metabolites indicates active secretion and extracellular transport of phenolic compounds, constituting a key component of chemical defense during the host–pathogen interaction [43]. The concurrent upregulation of lignin biosynthesis enzymes supports the deposition of phenolic polymers, strengthening cell wall integrity, while increased flavonoid production likely contributes to ROS scavenging and inhibition of fungal growth. Hormone-associated regulation, particularly via ethylene (ET), and JA signaling, may further modulate these secondary metabolic defenses [44]. Overall, activation of phenylpropanoid and flavonoid metabolism constitutes a central biochemical defense route in *A. squamosa*, integrating secondary metabolism and hormone signaling to enhance resistance.

4.5. Pathogen-Derived Protein Expression During Infection

Proteomic profiling revealed that *F. acutatum* undergoes substantial metabolic and structural reprogramming during infection, consistent with its transition from colonization to active tissue degradation (Figure 9 and Table S3). Among the 50 significantly altered fungal proteins, upregulation of ribosomal structural components (RPL13A, RPS7, etc.) reflects increased translational activity supporting rapid fungal proliferation and virulence factor synthesis during host colonization. Concurrent elevation of metabolic enzymes involved in central carbon metabolism, such as gabD, TPI, and ENO, suggests elevated glycolytic and energy-generating activity, which likely supports increased biosynthetic demands and hyphal expansion within host tissues [45]. *Fusarium* fungi can damage root structures by secreting CWDEs such as pectinase and cellulase, and inhibit host immunity by producing toxins like deoxynivalenol. The pronounced activation of multiple CWDEs, including exoglucanase, pectate lyase, β-glucosidase, and α-N-arabinofuranosidase, highlights a potential pathogenic strategy of *F. acutatum* that may involve enzymatic degradation of plant cell wall polysaccharides [46,47]. Such enzymes facilitate host penetration, nutrient acquisition, and systemic spread, consistent with the extensive root necrosis observed in infected *A. squamosa*. The concurrent enrichment of oxidoreductases and hydrolases

suggests that fungal oxidative metabolism and enzymatic breakdown are co-regulated processes contributing to virulence. Similar patterns have been reported in *F. oxysporum* and *F. graminearum*, where CWDEs and redox-active enzymes act synergistically to weaken host structural barriers and modulate defense-related reactive oxygen species (ROS) signaling [48,49]. Notably, catalase-peroxidase induction may reflect a potential fungal defense mechanism against host-derived oxidative bursts [50]. This enzyme could protect hyphae from host-generated H_2O_2, thereby maintaining pathogen viability within the oxidative environment of infected roots [51]. In parallel, the upregulation of NADP-specific glutamate dehydrogenase and isocitrate lyase implies activation of the glyoxylate cycle and nitrogen metabolism, which are critical for fungal adaptation under host-imposed nutrient limitation [52]. These metabolic adjustments likely enable *F. acutatum* to sustain infection by efficiently utilizing plant-derived substrates. Moreover, the identification of three hypothetical proteins as potential effectors, together with calmodulin, classified as a toxin-related protein, further suggests that *F. acutatum* may manipulate host defense signaling through secreted virulence factors. Calmodulin has been implicated in calcium-dependent signal transduction in several *Fusarium* species, regulating hyphal growth, sporulation, and stress tolerance [53,54]. The putative effectors (FOXG_02605, FOMG_08942, and FOXB_10756) may function in host immune suppression, cell wall integrity interference, or modulation of hormone signaling, warranting further characterization through host–pathogen co-localization and transient expression assays. Collectively, these findings delineate a coordinated virulence network in *F. acutatum*, integrating metabolic reprogramming, oxidative stress tolerance, and cell wall degradation with the potential deployment of secreted effectors and toxins. Such multifaceted adaptation underlies its efficient colonization of *A. squamosa* roots and highlights potential candidate targets for future resistance breeding.

4.6. Study Limitations

Despite morphological and ITS-based separation of the pathogen, species identification in this study relied solely on the ITS region, which may have limited resolution for closely related *Fusarium* species. Additional loci, such as *tef1* and *rpb2*, could provide more robust taxonomic confirmation [55,56]. Moreover, this study focused on two infection time points and a sample size sufficient for omics analyses, but these factors may limit detection of low-abundance unigenes or proteins, especially fungal proteins. While the pathogen was not re-isolated to formally fulfill Koch's postulates, and the functional contributions of several key host defense modules and fungal pathogenicity factors require further experimental validation. Addressing these limitations in future work will further strengthen understanding of *A. squamosa* defense mechanisms and improve the robustness of multi-omics inferences.

5. Conclusions

This multi-omics investigation outlines a comprehensive defense model of *A. squamosa* against *F. acutatum*. The host initiates rapid signaling cascades integrating redox regulation, phenylpropanoid metabolism, protein homeostasis, and structural reinforcement, while the pathogen concurrently reprograms its metabolism and virulence systems to sustain infection. The interplay between these adaptive processes defines the dynamic equilibrium of host resistance and pathogen aggression. This study provides multi-omics insights into *A. squamosa* defense against *F. acutatum* and highlights candidate targets supported by omics evidence, offering a theoretical reference for root rot management.

Supplementary Materials: The following supporting information can be downloaded at: https://www.mdpi.com/article/10.3390/horticulturae12010039/s1, Table S1: BLAST analysis of the ITS sequence. Table S2: Clean reads QC of transcription. Table S3: List of 50 *Fusarium*-derived proteins were significantly altered in LR vs. CK. Figure S1: GO and KEGG analysis of DEGs. (A) GO_CC statistics and enrichment of DEGs in the MR vs. CK comparison. (B) GO_CC statistics and enrichment of DEGs in the LR vs. CK comparison. (C) GO_BP statistics and enrichment of DEGs in the MR vs. CK comparison. (D) GO_BP statistics and enrichment of DEGs in the LR vs. CK comparison. (E) KEGG pathway statistics of DEGs in the MR vs. CK comparison. (F) KEGG pathway statistics of DEGs in the LR vs. CK comparison. Figure S2: GO and KEGG enrichment of DEPs. (A) GO enrichment analysis of DEPs in the MR vs. CK comparison and the Top 20 most significantly enriched GO terms. (B) GO enrichment analysis of DEPs in the LR vs. CK comparison and the Top 20 most significantly enriched GO terms. (C) KEGG enrichment of DEPs in MR vs. CK. (D) KEGG pathway statistics for MR vs. CK. (E) KEGG enrichment of DEPs in LR vs. CK. (F) KEGG pathway statistics for LR vs. CK. Figure S3: MapMan mapping of biotic stress. (A) DEPs mapped in MR vs. CK. (B) DEPs mapped in LR vs. CK. Figure S4: Changes in phenylpropanoid and flavonoid metabolism during infection. (A) DEPs mapped in secondary metabolism in MR vs. CK. (B) DEPs mapped in secondary metabolism in LR vs. CK. (C) DEPs mapped in phenylpropanoid metabolism in MR vs. CK. (D) DEPs mapped in phenylpropanoid metabolism in LR vs. CK. (E) qPCR validation of *CHI*, *CHS* and *CYP* genes.

Author Contributions: Conceptualization, Z.A.; Methodology, Z.A., R.K., X.L., Y.W. and J.Y.; Software, K.Y.; Formal analysis, S.L., Y.Q., J.T. and F.K.; Investigation, Z.A. and R.K.; Resources, W.T. and W.H.; Data curation, Z.A., R.K. and J.Z.; Writing—original draft, Z.A. and R.K.; Writing—review & editing, Z.A., R.K. and R.F.; Visualization, K.Y.; Supervision, J.Z. and R.F.; Funding acquisition, R.F. All authors have read and agreed to the published version of the manuscript.

Funding: This research was funded by the Guangxi Natural Science Foundation Project (2020GXNSFAA297073), Guangxi Academy of Agricultural Sciences, Science and Technology Development Fund (YYSZL2024002), Guangzhou Science and Technology Program Project (2025D04J0040), Guangxi Academy of Agricultural Sciences, Basic Scientific Research Business Special Project (Gui Nong Ke 2021YT049), and the Science and Technology Pioneer Team's Strong Agriculture, Enrich the People "Six One" Special Project (Gui Nong Ke Meng 202504).

Data Availability Statement: The transcriptome raw data are available via NCBI-SRA database with the accession PRJNA1378354. Proteomic raw data are available via ProteomeXchange with identifier PXD071733.

Conflicts of Interest: Author Shuhuan Lin was employed by the company Zhejiang Xinong Chemical Sales Co., Ltd. The remaining authors declare that the research was conducted in the absence of any commercial or financial relationships that could be construed as a potential conflict of interest.

References

1. Shaikh, N.M.; Muzammil, S.; Ali, S.M.S. A review on *Annona squamosa* L. *Int. J. Res. Pharm. Allied Sci.* **2025**, *4*, 56–65. [CrossRef]
2. Liu, K.D.; Li, H.L.; Yuan, C.C.; Huang, Y.L.; Chen, Y.; Liu, J.X. Identification of phenological growth stages of sugar apple (*Annona squamosa* L.) using the extended BBCH-scale. *Sci. Hortic.* **2015**, *181*, 76–80. [CrossRef]
3. Wang, Y.B.; Wang, W.H.; Liu, X.W.; Chen, M.H.; Jiang, J.X.; An, F.Q. Analysis of inter-root soil habitat and physiological traits in healthy and root rot-infested custard apple (*Annona Squamosa* L.) plants. *J. Soil Sci. Plant Nut.* **2025**, *25*, 3484–3497. [CrossRef]
4. Zhu, L.W.; Tang, X.M.; Lin, T.Y.; Zhou, S.S.; Liu, P.; Ye, Z.F.; Wang, D.S.; Wu, Z.Y. First report of *Fusarium* root rot in Asian pear caused by *Fusarium solani* in China. *Plant Dis.* **2017**, *101*, 252. [CrossRef]
5. Zakaria, L. Species associated with diseases of major tropical fruit crops. *Horticulturae* **2023**, *9*, 322. [CrossRef]
6. Zhan, R.L.; Lei, X.T.; He, Y.B.; Zhao, Y.L. Identification of root rot diseases and screening of biocontrol fungi in sugar apple. *J. Fruit. Sci.* **2005**, *22*, 234–237.
7. Zehra, A.; Meena, M.; Dubey, M.K.; Aamir, M.; Upadhyay, R.S. Synergistic effects of plant defense elicitors and *Trichoderma harzianum* on enhanced induction of antioxidant defense system in tomato against *Fusarium* wilt disease. *Bot. Stud.* **2017**, *58*, 44. [CrossRef]
8. Mohammadi, M.A.; Cheng, Y.; Aslam, M.; Jakada, B.H.; Wai, M.H.; Ye, K.Z.; He, X.X.; Luo, T.T.; Ye, L.; Dong, C.X.; et al. ROS and oxidative response systems in plants under biotic and abiotic stresses: Revisiting the crucial role of phosphite triggered plants defense response. *Front. Microbiol.* **2021**, *12*, 631318. [CrossRef]

9. Yang, J.; Zhang, Y.X.; Jia, J.T.; Wang, C.L.; Fu, Y.J. Flavonoid-lignin crosstalk: Engineering metabolic flux for optimised plant growth and stress resilience. *Plant Cell Environ.* **2025**, *48*, 8141–8160. [CrossRef] [PubMed]
10. Li, H.W.; Chen, N.N.; Zhang, H.B.; Xu, D.L. Multidimensional regulation of transcription factors: Decoding the comprehensive signals of plant secondary metabolism. *Front. Plant Sci.* **2025**, *16*, 1522278. [CrossRef]
11. Matic, S.; Bagnaresi, P.; Biselli, C.; Orru, L.; Carneiro, G.A.; Siciliano, I.; Valé, G.; Gullino, M.L.; Spadaro, D. Comparative transcriptome profiling of resistant and susceptible rice genotypes in response to the seedborne pathogen *Fusarium fujikuroi*. *BMC Genom.* **2016**, *17*, 608. [CrossRef]
12. Gu, S.; Zhao, C.; Xie, L.; Sheng, X.R.; Xing, G.Q.; Zhou, J.X.; Wang, X.Y. Roles of ethylene and abscisic acid produced by *Alternaria alternata* and *Fusarium fujikuroi* in postharvest disease of blueberries. *J. Agric. Food Chem.* **2025**, *73*, 17421–17431. [CrossRef]
13. Zielinska, M.; Michniewicz, M. The effect of calcium on the production of ethylene and abscisic acid by fungus *Fusarium culmorum* and by wheat seedlings infected with that pathogen. *Acta Physiol. Plant.* **2001**, *23*, 79–85. [CrossRef]
14. Li, J.; Feng, L.D.; Li, D.; Liu, X.L.; Pan, Y.Y.; He, J.; Zhang, J.X. ROS Regulate NCF2, Key metabolic enzymes and MDA levels to affect the growth of *Fusarium solani*. *Agriculture* **2022**, *12*, 1840. [CrossRef]
15. Lionetti, V.; Giancaspro, A.; Fabri, E.; Giove, S.L.; Reem, N.; Zabotina, O.A.; Blanco, A.; Gadaleta, A.; Bellincampi, D. Cell wall traits as potential resources to improve resistance of durum wheat against *Fusarium graminearum*. *BMC Plant Biol.* **2015**, *15*, 6. [CrossRef]
16. Wu, Y.L.; Yi, G.J.; Peng, X.X.; Huang, B.Z.; Liu, E.; Zhang, J.J. Systemic acquired resistance in Cavendish banana induced by infection with an incompatible strain *Fusarium oxysporum* f. sp. *cubense*. *J. Plant Physiol.* **2013**, *170*, 1039–1046. [CrossRef]
17. Gautam, R.; Singh, S.K.; Sharma, V. Molecular diagnosis and intraspecific genetic variability of root pathogens of arid legumes in Western Rajasthan, India. *Rev. Biol. Trop.* **2016**, *64*, 1505–1518. [CrossRef]
18. Dutta, R.; Jayalakshmi, K.; Radhakrishna, A.; Kumar, S.; Mahajan, V. Active prevalence of *Fusarium falciforme* and *F. acutatum* causing basal rot of onion in Maharashtra, India. *J. Fungi* **2024**, *10*, 413. [CrossRef]
19. *NY/T 2054-2011*; Technical Code for Evaluating Disease Resistance of Annona. Ministry of Agriculture of the People's Republic of China: Beijing, China, 2011.
20. Jiang, N.; Lin, B.R.; Song, L.S.; Tan, G.Y.; Zhang, Z.J.; Yu, K. Integrated transcriptome and proteome analyses unravel a series of early defence responses in *Sarcandra glabra* against *Colletotrichum gloeosporioides*. *Funct. Plant Biol.* **2023**, *50*, 1047–1061. [CrossRef] [PubMed]
21. Lohse, M.; Nagel, A.; Herter, T.; May, P.; Schroda, M.; Zrenner, R.; Tohge, T.; Fernie, A.R.; Stitt, M.; Usadel, B. Mercator: A fast and simple web server for genome scale functional annotation of plant sequence data. *Plant Cell Environ.* **2014**, *37*, 1250–1258. [CrossRef]
22. Savojardo, C.; Martelli, P.L.; Fariselli, P.; Casadio, R. DeepSig: Deep learning improves signal peptide detection in proteins. *Bioinformatics* **2018**, *34*, 1690–1696. [CrossRef]
23. Liu, S.S.; Yang, S.; Liu, H.Z.; Hu, Q.D.; Liu, X.; Wang, J.W.; Wang, J.Y.; Xin, W.Z.; Chen, Q.X. Physiological and transcriptomic analysis of the mangrove species *Kandelia obovata* in response to flooding stress. *Mar. Pollut. Bull.* **2023**, *196*, 115598. [CrossRef]
24. Amobonye, A.; Bhagwat, P.; Ranjith, D.; Mohanlall, V.; Pillai, S. Characterisation, pathogenicity and hydrolytic enzyme profiling of selected *Fusarium* species and their inhibition by novel coumarins. *Arch. Microbiol.* **2021**, *203*, 3495–3508. [CrossRef]
25. Deenamo, N.; Kuyyogsuy, A.; Khompatara, K.; Chanwun, T.; Ekchaweng, K.; Churngchow, N. Salicylic acid induces resistance in rubber tree against *Phytophthora palmivora*. *Int. J. Mol. Sci.* **2018**, *19*, 1883. [CrossRef] [PubMed]
26. Onkokesung, N.; Gális, I.; von Dahl, C.C.; Matsuoka, K.; Saluz, H.P.; Baldwin, I.T. Jasmonic acid and ethylene modulate local responses to wounding and simulated herbivory in *Nicotiana attenuata* leaves. *Plant Physiol.* **2010**, *153*, 785–798. [CrossRef] [PubMed]
27. Gruner, K.; Griebel, T.; Návarová, H.; Attaran, E.; Zeier, J. Reprogramming of plants during systemic acquired resistance. *Front. Plant Sci.* **2013**, *4*, 252. [CrossRef] [PubMed]
28. Kumar, R.; Singh, A.; Shukla, E.; Singh, P.; Khan, A.; Singh, N.K.; Srivastava, A. Siderophore of plant growth promoting rhizobacterium origin reduces reactive oxygen species mediated injury in *Solanum* spp. caused by fungal pathogens. *J. Appl. Microbiol.* **2024**, *135*, lxae036. [CrossRef]
29. Fuertes-Rabanal, M.; Largo-Gosens, A.; Fischer, A.; Munzert, K.S.; Carrasco-López, C.; Sánchez-Vallet, A.; Engelsdorf, T.; Mélida, H. Linear β-1,2-glucans trigger immune hallmarks and enhance disease resistance in plants. *J. Exp. Bot.* **2024**, *75*, 7337–7350. [CrossRef]
30. Aybeke, M. Fusarium infection causes genotoxic disorders and antioxidant-based damages in *Orobanche* spp. *Microbiol. Res.* **2017**, *201*, 46–51. [CrossRef]
31. Sahu, A.K.; Kumari, P.; Mittra, B. Immunocompromisation of wheat host by L-BSO and 2,4-DPA induces susceptibility to the fungal pathogen *Fusarium oxysporum*. *Stress Biol.* **2024**, *4*, 21. [CrossRef]
32. Taheri, P.; Tarighi, S. Riboflavin induces resistance in rice against *Rhizoctonia solani* via jasmonate-mediated priming of phenylpropanoid pathway. *J. Plant Physiol.* **2010**, *167*, 201–208. [CrossRef]
33. Liu, Y.A.; Jackson, E.; Liu, X.R.; Huang, X.C.; van der Hoorn, R.A.L.; Zhang, Y.L.; Li, X. Proteolysis in plant immunity. *Plant Cell* **2024**, *36*, 3099–3115. [CrossRef] [PubMed]
34. Sun, J.L.; Li, J.Y.; Wang, M.J.; Song, Z.T.; Liu, J.X. Protein quality control in plant organelles: Current progress and future perspectives. *Mol. Plant* **2021**, *14*, 95–114. [CrossRef]

35. Sami, F.; Siddiqui, H.; Alam, P.; Hayat, S. Glucose-induced response on photosynthetic efficiency, ROS homeostasis, and antioxidative defense system in maintaining carbohydrate and ion metabolism in Indian mustard (*Brassica juncea* L.) under salt-mediated oxidative stress. *Protoplasma* **2021**, *258*, 601–620. [CrossRef]
36. Ninkuu, V.; Yan, J.P.; Zhang, L.; Fu, Z.C.; Yang, T.F.; Li, S.P.; Li, B.B.; Duan, J.Q.; Ren, J.; Li, G.Y.; et al. Hrip1 mediates rice cell wall fortification and phytoalexins elicitation to confer immunity against. *Front. Plant Sci.* **2022**, *13*, 980821. [CrossRef]
37. Ninkuu, V.; Aluko, O.O.; Yan, J.P.; Zeng, H.M.; Liu, G.D.; Zhao, J.; Li, H.H.; Chen, S.B.; Dakora, F.D. Phenylpropanoids metabolism: Recent insight into stress tolerance and plant development cues. *Front. Plant Sci.* **2025**, *16*, 1571825. [CrossRef]
38. Rigano, D.; Formisano, C.; Basile, A.; Lavitola, A.; Senatore, F.; Rosselli, S.; Brtmo, M. Antibacterial activity of flavonoids and phenylpropanoids from *Marrubium globosum* ssp. *libanoticum*. *Phytother. Res.* **2007**, *21*, 395–397. [CrossRef]
39. Sun, T.R.; Yang, W.T.; Zhang, W.D.; Liu, Y.X.; Li, L.L.; Cheng, S.B.; Chen, G.G. Phenylpropanoid pathway mediated the defense response of 'Korla' fragrant pear against *Alternaria alternata* infection. *Postharvest Biol. Tec.* **2025**, *220*, 113318. [CrossRef]
40. Xiao, J.C.; Cao, B.Y.; Tang, W.; Sui, X.Y.; Tang, Y.; Lai, Y.S.; Sun, B.; Huang, Z.; Zheng, Y.X.; Li, H.X. The CaCAD1-CaPOA1 module positively regulates pepper resistance to cold stress by increasing lignin accumulation. *Int. J. Biol. Macromol.* **2025**, *290*, 139979. [CrossRef]
41. Kundu, P.; Shinde, S.; Grover, S.; Sattler, S.E.; Louis, J. Caffeic acid O-methyltransferase-dependent flavonoid defenses promote sorghum resistance to fall armyworm infestation. *Plant Physiol.* **2025**, *197*, kiaf071. [CrossRef] [PubMed]
42. Wang, M.L.; Wang, Y.D.; Li, X.Z.; Zhang, Y.; Chen, X.L.; Liu, J.Y.; Qiua, Y.; Wang, A.X. Integration of metabolomics and transcriptomics reveals the regulation mechanism of the phenylpropanoid biosynthesis pathway in insect resistance traits in Solanum habrochaites. *Hortic. Res.* **2024**, *11*, uhad277. [CrossRef]
43. Hassan, S.; Mathesius, U. The role of flavonoids in root-rhizosphere signalling: Opportunities and challenges for improving plant-microbe interactions. *J. Exp. Bot.* **2012**, *63*, 3429–3444. [CrossRef]
44. Silva, L.F.; Barreto, K.F.M.; Silva, H.C.; de Souza, I.D.; Meneses, C.H.S.G.; Uchôa, A.F.; Scortecci, K.C. Insights of cellular and molecular changes in sugarcane response to oxidative signaling. *BMC Plant Biol.* **2025**, *25*, 54. [CrossRef]
45. Li, J.J.; Chroumpi, T.; Garrigues, S.; Kun, R.S.; Meng, J.L.; Salazar-Cerezo, S.; Aguilar-Pontes, M.V.; Zhang, Y.; Tejomurthula, S.; Lipzen, A.; et al. The sugar metabolic model of *Aspergillus niger* can only be reliably transferred to fungi of its phylum. *J. Fungi* **2022**, *8*, 1315. [CrossRef] [PubMed]
46. Rafiei, V.; Vélëz, H.; Tzelepis, G. The role of glycoside hydrolases in phytopathogenic fungi and oomycetes virulence. *Int. J. Mol. Sci.* **2021**, *22*, 9359. [CrossRef] [PubMed]
47. Kim, J.Y.; Wu, J.N.; Kwon, S.J.; Oh, H.; Lee, S.E.; Kim, S.G.; Wang, Y.M.; Agrawal, G.K.; Rakwal, R.; Kang, K.Y.; et al. Proteomics of rice and *Cochliobolus miyabeanus* fungal interaction: Insight into proteins at intracellular and extracellular spaces. *Proteomics* **2014**, *14*, 2307–2318. [CrossRef]
48. Günther, K.L. Investigation of the Reactive Oxygen Species Metabolism During the Life Cycle of *Fusarium graminearum*. Doctoral Dissertation, Staats-und Universitätsbibliothek Hamburg Carl von Ossietzky, Hamburg, Germany, 2018.
49. Feng, L.; Zhao, G.J.; Sun, R.; Wang, J.F.; Sun, T.X.; Xing, S.Y.; Lian, W.H.; Zhao, Y. Dynamic changes in cell wall-degrading enzymes and physio-biochemistry of ginseng in response to *Fusarium oxysporum* infection. *Eur. J. Plant Pathol.* **2023**, *165*, 569–578. [CrossRef]
50. Zhang, J.; Li, H.M.; Gu, W.L.; Zhang, K.X.; Liu, X.Y.; Liu, M.X.; Yang, L.Y.; Li, G.; Zhang, Z.G.; Zhang, H.F. Peroxisome dynamics determines host-derived ROS accumulation and infectious growth of the rice blast fungus. *mBio* **2023**, *14*, e02381-23. [CrossRef]
51. Tanabe, S.; Ishii-Minami, N.; Saitoh, K.I.; Otake, Y.; Kaku, H.; Shibuya, N.; Nishizawa, Y.; Minami, E. The role of catalase-peroxidase secreted by *Magnaporthe oryzae* during early infection of rice cells. *Mol. Plant-Microbe Interact.* **2011**, *24*, 163–171. [CrossRef]
52. Gálvez, S.; Gadal, P. On the function of the NADP-dependent isocitrate dehydrogenase isoenzymes in living organisms. *Plant Sci.* **1995**, *105*, 1–14. [CrossRef]
53. Hou, Y.H.; Hsu, L.H.; Wang, H.F.; Lai, Y.H.; Chen, Y.L. Calcineurin regulates conidiation, chlamydospore formation and virulence in *Fusarium oxysporum* f. sp. *lycopersici*. *Front. Microbiol.* **2020**, *11*, 539702. [CrossRef] [PubMed]
54. Lange, M.; Peiter, E. Calcium transport proteins in fungi: The phylogenetic diversity of their relevance for growth, virulence, and stress resistance. *Front. Microbiol.* **2020**, *10*, 3100. [CrossRef]
55. Yassin, Z.; Salehi, Z.; Soleimani, M.; Lotfali, E.; Fattahi, M.; Sharifynia, S. Phylogenetic relationship of *Fusarium* species isolated from keratitis using TEF1 and RPB2 gene sequences. *Iran. J. Microbiol.* **2022**, *14*, 417–422. [CrossRef] [PubMed]
56. Gao, Y.; Zhang, Z.; Ji, M.; Ze, S.; Wang, H.; Yang, B.; Hu, L.; Zhao, N. Identification and pathogenicity of *Fusarium* species from herbaceous plants on grassland in Qiaojia County, China. *Microorganisms* **2025**, *13*, 113. [CrossRef] [PubMed]

Disclaimer/Publisher's Note: The statements, opinions and data contained in all publications are solely those of the individual author(s) and contributor(s) and not of MDPI and/or the editor(s). MDPI and/or the editor(s) disclaim responsibility for any injury to people or property resulting from any ideas, methods, instructions or products referred to in the content.